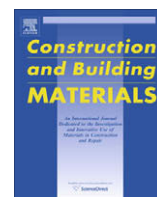




Contents lists available at ScienceDirect

# Construction and Building Materials

journal homepage: [www.elsevier.com/locate/conbuildmat](http://www.elsevier.com/locate/conbuildmat)

## Combined use of thermography and ultrasound for the characterization of subsurface cracks in concrete

D.G. Aggelis\*, E.Z. Kordatos, D.V. Soulioti, T.E. Matikas

Department of Materials Science and Engineering, University of Ioannina, 45110 Ioannina, Greece

### ARTICLE INFO

#### Article history:

Received 2 December 2009

Received in revised form 26 February 2010

Accepted 1 April 2010

Available online 21 April 2010

#### Keywords:

Corrosion cracking  
Thermography  
Ultrasound

### ABSTRACT

Corrosion of metal reinforcement in concrete structures leads to cracks extending towards the surface. These cracks do not show any visual sign until they break the surface, exposing the structure to more accelerated deterioration. In order to develop a methodology for subsurface damage characterization, a combination of nondestructive testing (NDT) techniques was applied. Thermography is specialized in subsurface damage identification due to anomalies that inhomogeneities impose on the temperature field. Additionally, ultrasonic Rayleigh waves are constrained near the surface and therefore, are ideal for characterization of near-surface damage. In this study, an infrared camera scans the specimen in order to indicate the position of the crack. Consequently, ultrasonic sensors are placed on the specified part of the surface in order to make a more detailed assessment for the depth of the crack. Although there is no visual sign of damage, Rayleigh waves are influenced in terms of velocity and attenuation. Numerical simulations are also conducted, to propose suitable parameters like frequency for more accurate testing. The combination of the NDT techniques seems promising for real structures assessment.

© 2010 Elsevier Ltd. All rights reserved.

### 1. Introduction

The deterioration of civil infrastructure calls for effective methods of monitoring and repair. The maintenance procedure usually employs a combination of techniques [1]. First a global monitoring technique for the general assessment of the structure in a time efficient manner is applied. The results indicate the severity of the condition and localize the specific parts of the structure which require more detailed examination. Consequently, another technique can be applied locally at the specified positions for a more accurate characterization of the damage parameters [2].

Subsurface cracking in concrete structures may occur due to corrosion of reinforcement if environmental agents penetrate into the material [3]. The layer of oxides formed on the bar, applies additional stresses in the concrete matrix, resulting in its cracking. These cracks propagate with the increase of corrosion, as well as due to thermal cycles and external loading (see Fig. 1). However, they are not visible until they break the surface. Therefore, their assessment by visual inspection is not possible until late. When they break the surface they accelerate the deterioration through the direct channel the crack supplies to water penetration in the structure. It is reasonable that an NDT methodology is demanded for the early assessment of the material's condition in order for

the engineers to take the proper action, which could be epoxy or cement injection at the specific position in order to seal the crack [4]. In the present case, this is attempted by the combination of thermography, used as a global monitoring tool to indicate the possible areas of subsurface defects and one-sided ultrasonic propagation, parameters of which are influenced mainly by the depth of damage on the specified areas.

The application of infrared thermography in civil engineering is an established nondestructive method for economical, accurate and convenient investigation of the quality of insulation of buildings, heat loss through windows, or "hidden details" like subsurface defects and delaminations [5–8]. The heat rate is influenced by the presence of defects inside the mass of concrete. This influence may be projected to the surface by variations of the temperature distribution. The variation is stronger as the defects are closer to the surface. Cameras collect infrared radiation emitted by the surface, convert it into electrical signals and create a thermal image showing the body's surface temperature distribution. This distribution is influenced by the existence of subsurface inhomogeneities which leave their fingerprint on the surface temperature field.

Concerning elastic waves, their parameters such as wave speed and transmission in general are influenced by the existence of damage [9]. As long as one-sided measurements are concerned, the propagation velocities of longitudinal and Rayleigh waves decrease for damaged material, while the attenuation coefficient increases mainly due to scattering [10]. Elastic waves have been

\* Corresponding author. Tel.: +30 26510 08006; fax: +30 26510 08054.  
E-mail address: [daggelis@cc.uoi.gr](mailto:daggelis@cc.uoi.gr) (D.G. Aggelis).

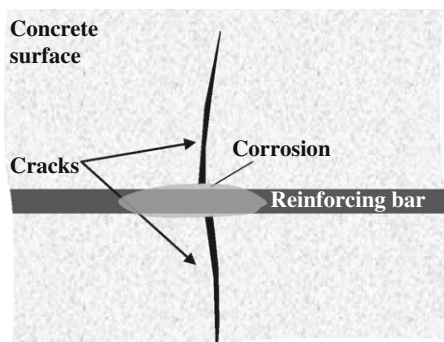


Fig. 1. Development of subsurface cracks by corrosion of rebar.

investigated for the detection of surface and near-surface cracks, showing mainly that their amplitude and frequency is influenced by the existence of damage [11–14]. Therefore, the interaction between subsurface cracks and wave parameters obtained by one-sided measurements are of considerable interest.

In the present study, steel fiber-reinforced concrete prism specimens were subjected to four-point bending. This resulted in visible cracks propagating from the bottom, tensile side to the top. Due to the fiber action, the specimens were not separated in two parts and the crack was halted before reaching the compression side. An infrared camera was used to scan this side of the specimens at the cooling down stage after heating in an oven. The specimens were also examined by one-sided elastic wave measurements by means of resonant acoustic emission sensors in order to estimate the influence of the crack on basic wave parameters. The specific elastic wave problem was also numerically modelled in order to expand to different frequencies and crack geometries and propose suitable experimental parameters for in situ use.

## 2. Materials

The specimens were made of steel fiber-reinforced concrete (SFRC). Their size was  $100 \times 100 \times 400$  mm. The water to cement ratio by mass was 0.5 and the aggregate to cement ratio 5. The maximum aggregate size was 10 mm. The fiber contents were 0.5%, 1% and 1.5% by volume. Additionally, plain concrete specimens were cast. The specimens were tested in four-point bending for fracture toughness determination (ASTM C1609/C 1609M-05) resulting in approximately vertical cracks which propagated from the bottom tensile surface to the top (see Fig. 2a). Fig. 2b shows a typical crack in SFRC specimen. The main crack is accompanied by smaller cracks, as is typical for this kind of material, increasing the fracture process zone. Despite the network of cracks, which can be seen from the side view, there is no visible sign of them from the compression side. More details on the specimens' composition can be seen in another study [15].

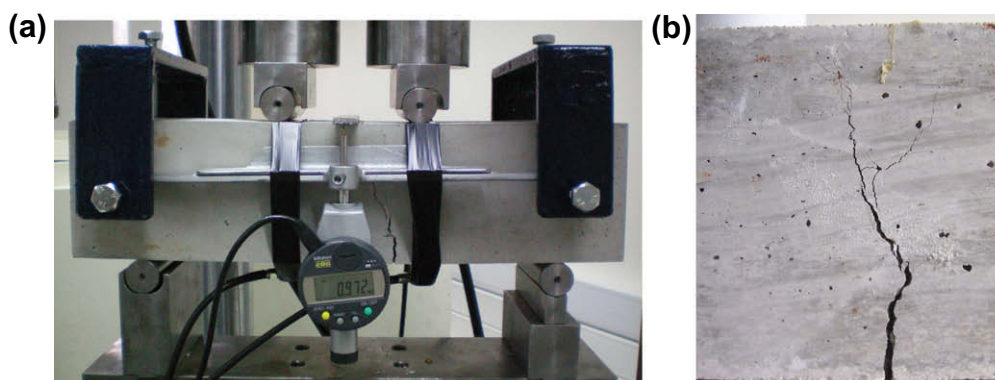


Fig. 2. (a) Experimental setup for four-point bending and (b) typical crack in SFRC.

## 3. Ultrasonic measurements

### 3.1. Experimental setup

The experimental setup for the elastic wave measurements is depicted in Fig. 3. Two sensors were placed on the intact side of the specimen at a distance of 70 mm. The excitation was conducted by pencil lead break which introduces a frequency band up to approximately 200 kHz. The sensors were common acoustic emission transducers (Physical Acoustics, PAC R6), with nominal maximum sensitivity around 60 kHz with very good response up to 150 kHz, and diameter of 15 mm. The sampling frequency of the acquisition board was set to 5 MHz. This kind of ultrasonic set up is commonly used in monitoring of concrete structures [4,10].

Wave velocity was measured by the time delay between the waveforms collected at the different sensors. Typical waveforms recorded on sound material are depicted in Fig. 4a. For pulse velocity determination the first disturbances (wave onsets in Fig. 4a) were used. The onset corresponds to the longitudinal wave which is the fastest type. Rayleigh wave velocity was measured by the strong characteristic peaks (see again Fig. 4a) of the Rayleigh waves which stand higher than the initial longitudinal arrivals due to their higher energy [16]. Fig. 4b shows typical waveforms for the case of a subsurface cracked concrete specimen. The waveform of the 1st receiver is similar to the intact case; however, the waveform recorded by the second receiver is much lower in amplitude and therefore for presentation purposes it is magnified by 80 in the figure. In some cases with severe cracking it was difficult to discriminate the Rayleigh peak. However, this shows that the crack has cut through the whole cross section. The measurements were repeated 20 times by slightly translating and rotating the receivers' array around the crack in order to study also the exper-

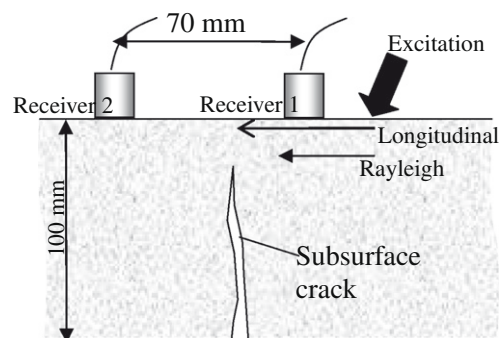


Fig. 3. Experimental setup for one-sided wave measurements.

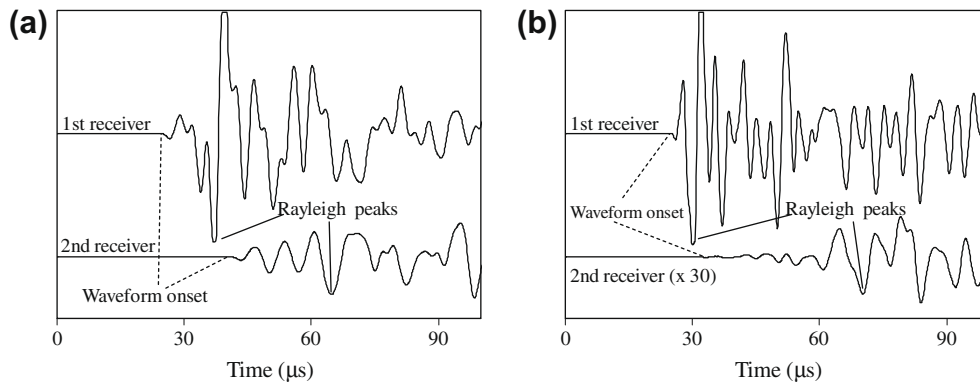


Fig. 4. Typical waveforms for (a) sound material and (b) subsurface cracked material.

imental scatter for sound and cracked material. The additional measurements take just a few minutes which is a minimal time span when the equipment is set. The wave propagation results were grouped in intact and cracked regardless of the fiber content of the specimens since its contribution was minimal compared to the effect of the crack.

3.2. Subsurface crack influence on wave parameters

The longitudinal wave velocities measured on healthy SFRC specimens averaged at 4307 m/s. The average velocity measured on the portion of the specimens with subsurface damage, decreased by more than 20% to 3304 m/s, as can be seen in Fig. 5. Rayleigh wave results were similar, since the velocity was decreased by 19% from 2231 to 1814 m/s. Apart from wave velocities another parameter which is very sensitive to damage is the attenuation which is connected to the amplitude of the waveforms. Due to different mechanisms such as absorption, scattering and geometric spreading, the 2nd receiver receives lower amplitude than the first. In addition to that, the existence of the subsurface crack, depending on its location, causes the reflection of a major part of the wave energy further reducing the amplitude on the second receiver. Considering the absolute maximum amplitude recorded by the 2nd receiver divided by the amplitude recorded by the 1st, the ratio is 0.335 for sound material. In the case of subsurface damage, this ratio decreases to 0.061, being reduced by more than 80% (see Fig. 5). This is another case that shows the high sensitivity of attenuation parameters to the existence of damage [17].

Complementary to the above, the experimental scatter of the measurements supplies additional information [18]. In concrete which is by nature inhomogeneous, different parts of the material include different aggregates, air bubbles, porosity, and therefore,

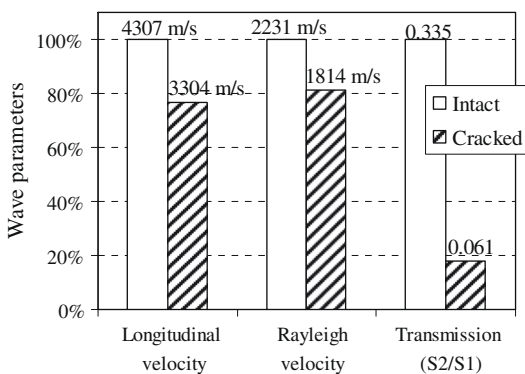


Fig. 5. Measured elastic wave parameters.

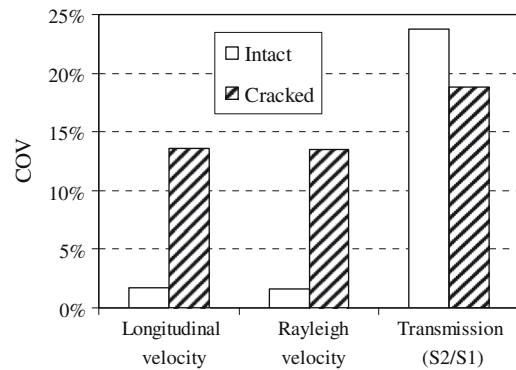


Fig. 6. COV for different elastic wave parameters.

taking a number of individual measurements will result in a slight statistical variation on the measured properties compared to the case of a more homogeneous material. Furthermore, in case of damaged concrete, the random shape of the cracks is expected to increase the variability. This is due to different parameters like the angle of wave incidence on the crack, and different crack-bridging points. Fig. 6 shows the experimental scatter, expressed by the coefficient of variation, COV (standard deviation divided by the average of 20 measurements). The experimental scatter for both longitudinal and Rayleigh is strongly increased for cracked material. The sound concrete exhibits very similar measurements with COV less than 3%. However, for the cracked concrete, COV is about 14%. On the other hand the COV of the amplitude measurements was already high enough (more than 20%). This is reasonable due to the known sensitivity of attenuation on the microstructure. Concerning the cracked material this parameter was slightly decreased. In general it can be said that when the equipment is set in the field for monitoring, instead of just one, a more representative number of measurements can be taken, providing another very sensitive-to-damage parameter; besides the velocity value drop which may be around 20%, as seen in Fig. 5, the scatter of the velocity measurements (COV) increases much more clearly (i.e. approximately 400%) when damaged material is examined.

4. Elastic wave simulation

Simulations enhance the understanding in wave propagation. Cases which are difficult or expensive to be examined experimentally can be studied through simulations. In the present case, the experiment was conducted by resonant sensors. Therefore, simulations are a means to expand to different frequencies. Additionally, although the bending experiments were conducted with displace-

ment control, there was no control on the length of the subsurface cracks developed. These cracks almost reached the opposite surface and thus, had a clear effect on the wave parameters. In order to examine different cases of subsurface crack depths of the order of some centimeters, numerical simulations were performed.

Commercial software was used [19]. It operates by solving the two-dimensional elastic wave equations based on a method of finite differences [20]. The material was considered elastic with no viscosity components. The Lamé constants were  $\lambda = 12$  GPa and  $\mu = 16.5$  GPa, with density of  $2400 \text{ kg/m}^3$ , resulting in a longitudinal wave velocity of  $4300 \text{ m/s}$  similar to the healthy SFR concrete. The corresponding elastic modulus is  $40 \text{ GPa}$  and Poisson's ratio  $0.2$ .

The geometric model was of rectangular shape with  $100 \text{ mm}$  thickness to resemble the experimental specimen, see Fig. 7a. The mesh size of the calculation was set to  $0.2 \text{ mm}$  much smaller than the longitudinal wavelength of  $43 \text{ mm}$ , and the Rayleigh of  $24 \text{ mm}$  ensuring accurate solution. In order to reduce the calculation time, the specimen's length was reduced to  $200 \text{ mm}$  and infinite boundary conditions were applied to the opposite sides, cancelling the reflections from the edges. The two simulated receivers were  $15 \text{ mm}$  long to resemble the actual transducers and were placed on the top side of the specimen with a separation of  $70 \text{ mm}$ . The receivers computed the average lateral displacement on their defined length. The simulated cases concerned the crack-free geometry as well as geometries with subsurface cracks. The intact layer between the surface and the crack (depth of crack) was varied, namely at  $60, 40, 20, 10, 8, 5, 3$  and  $1 \text{ mm}$ . The crack had a thickness of  $1 \text{ mm}$ . Fig. 7a shows the displacement field for the specimen with a subsurface crack  $40 \text{ mm}$  below the surface. The snapshot corresponds to time  $32 \mu\text{s}$  after the excitation of one cycle of  $100 \text{ kHz}$ . Fig. 7b shows the waveforms obtained after the completion of the simulation of this case. The characteristic Rayleigh cycle can be distinguished for both receivers. In the case of the 2nd receiver, the initial longitudinal arrivals are clearly seen before the Rayleigh cycle since the path is sufficiently long for the individual modes to be separated due to different velocities. The second strong cycle recorded by the first receiver (marked by an

asterisk) is the reflection of the longitudinal wave from the bottom side of the beam.

Fig. 7c shows the corresponding case of a subsurface crack,  $1 \text{ mm}$  below the surface, while the waveforms are included in Fig. 7d. Since the crack is close to the surface only a small amount of energy can propagate towards the 2nd receiver. The displacement field is distorted while the waveform of the 2nd receiver is much lower in amplitude since most of the energy is reflected back

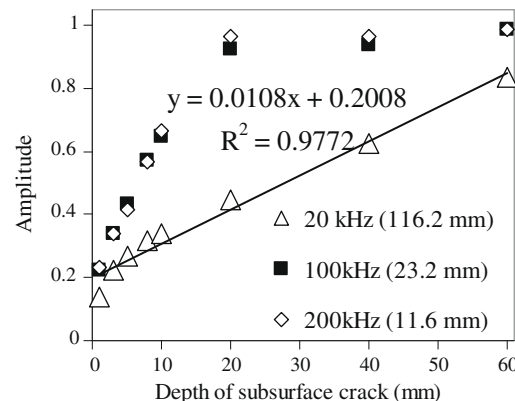


Fig. 8. Amplitude vs. depth of subsurface crack. (The number in parenthesis correspond to the wavelength.)

Table 1  
Main characteristics of the Flir T360 infrared camera.

Temperature range	−20 to 350 °C
Detector type – focal plane array	320 × 240 pixels – (FPA) uncooled microbolometer
Spectral range	7.5–13 μm
Thermal sensitivity	<0.06 °C at 30 °C
Accuracy	±2% of the measure
Field of view/min focus distance	25° × 19°/0.4 m

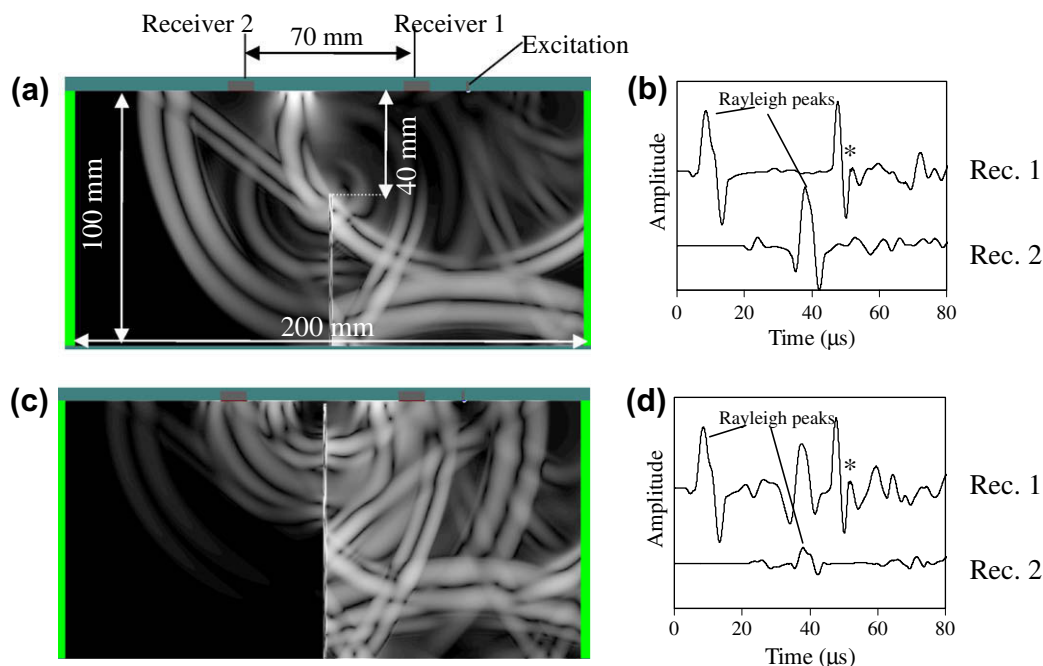


Fig. 7. (a) Snapshot of the displacement field for a specimen with a subsurface crack  $40 \text{ mm}$  below the surface and (c)  $1 \text{ mm}$  below the surface, (b) and (d) waveforms obtained for the simulation of (a) and (c) correspondingly. The excitation is one cycle of  $200 \text{ kHz}$ .

by the discontinuity. In any case the Rayleigh contribution is clear on both receivers and velocity measurements are enabled. The longitudinal reflection is again seen on the response of receiver 1, as well as another strong cycle earlier at approximately  $40 \mu\text{s}$ , which is the reflection of the Rayleigh on the crack. This reflection was not present in Fig. 7b because the depth to crack was long enough to allow most of the energy to propagate.

In order to study the wavelength influence, the frequency was varied. The change of frequency modifies also the depth of Rayleigh penetration. Three basic cases were examined, namely 100 kHz (similar to the experiment), 200 and 20 kHz to expand to shorter and longer wavelengths. The corresponding Rayleigh wavelengths were 23.2, 11.6 and 116.2 mm.

From the parameters examined, amplitude proved the most sensitive to the depth of the crack. It is briefly mentioned that P-wave velocity was hardly influenced even for the shallowest crack of 1 mm, while Rayleigh wave velocity exhibited a decrease of 5% when the low frequency of 20 kHz was applied. Fig. 8 shows the

amplitude of the 2nd receiver's waveform for different depths of crack after normalization to the amplitude of the 2nd receiver for sound material. The amplitude decreases strongly, especially for very shallow cracks reaching a value approximately 20% of the sound case. As the healthy part below the surface increases (the depth of crack increases), the amplitudes of the 100 and 200 kHz waves are restored to the reference level, meaning that these frequencies lose their sensitivity for cracks deeper than 20 mm (see Fig. 8). However, the amplitude of 20 kHz shows a slow rate of increase until even the subsurface crack of 60 mm depth. The amplitude vs. depth line can be roughly considered linear, showing that a positive estimation may be conducted based on the amplitude of the wave which proves to be the most sensitive parameter in order to characterize the depth of the crack. This is in accordance to the experimental measurements, which, as presented in Fig. 5, show that the amplitude of the wave is the most sensitive parameter to the underlying damage. Simulations for deeper cases were not conducted since the cracks considered in this case, originate from

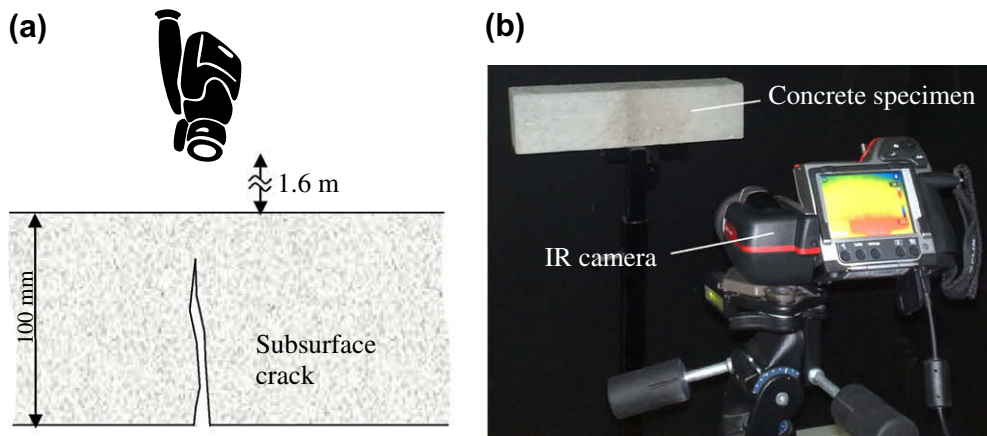


Fig. 9. Representation (a) and photograph (b) of the IR thermography experimental setup.

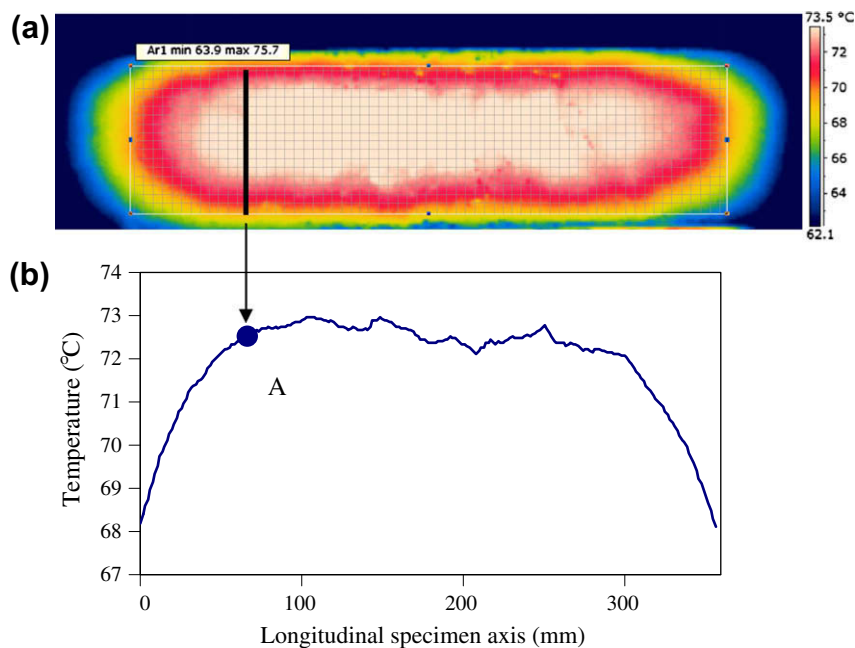


Fig. 10. (a) Thermograph of an intact specimen and (b) average temperature for the axis of specimen.

metal rebars embedded at approximately 50–60 mm below the surface.

From the above it is understandable that when a specific subsurface defect is targeted, the characterization of certain parameters like its depth, is possible using one-sided wave measurement. In a large structure though, since there is not always visual evidence of the damage lying beneath, there should be another method for the first scanning in order to reliably indicate the position where ultrasonic sensors should be used. For this role infrared thermography is applied, as explained below.

### 5. Thermography

The experimental setup constituted from an infrared camera and an oven. The infrared camera was the Flir T360. The main characteristics of the infrared camera are summarized in Table 1. The energy source employed for the heating of the specimens was an oven with temperature range 20–200 °C.

Four specimens were heated in an oven for 3 h at 90 °C. The infrared camera was placed at 1.6 m distance from the specimens, as seen in Fig. 9a and b. The thermal emissivity of concrete is 0.92 [6] and there was no need to paint the surface. Experiments were conducted in laboratory under constant conditions of air tempera-

ture of 23 °C and relative humidity 70%. Thermographs were recorded during the cooling stage of the specimens and some of the most indicative IR graphs for each specimen are presented in the next figures.

Fig. 10a shows the thermograph of a healthy specimen. The temperature field is homogeneous in the center of the specimen while there is accelerated cooling near the edges of the specimen. In order to enhance the detection, the scanned area was divided with a mesh size of 1.5 mm. This was done in order to obtain a deterministic parameter connected to the geometry of the specimen that indicates the position of the possible defect. Concrete usually has some visible surface defects like air bubbles that can act as temperature release points. Therefore, they are also captured by the infrared camera and may mislead the characterization. In order to reduce this possibility, the average temperature of the nodes of each vertical line of the mesh was calculated. A small surface defect like air bubble can locally change the temperature reading of only a few nodes. However, these nodes cannot change the average value of the vertical line which is made up by the temperature of 50 nodes. This average temperature line for the sound specimen is depicted in Fig. 10b. As an example, a specific point (e.g. A in Fig. 10b), is calculated as the average of all the points included in the corresponding vertical bold line of Fig. 10a. The temperature line remains approximately constant for the center of the specimen while closing at the edges it decreases smoothly. This

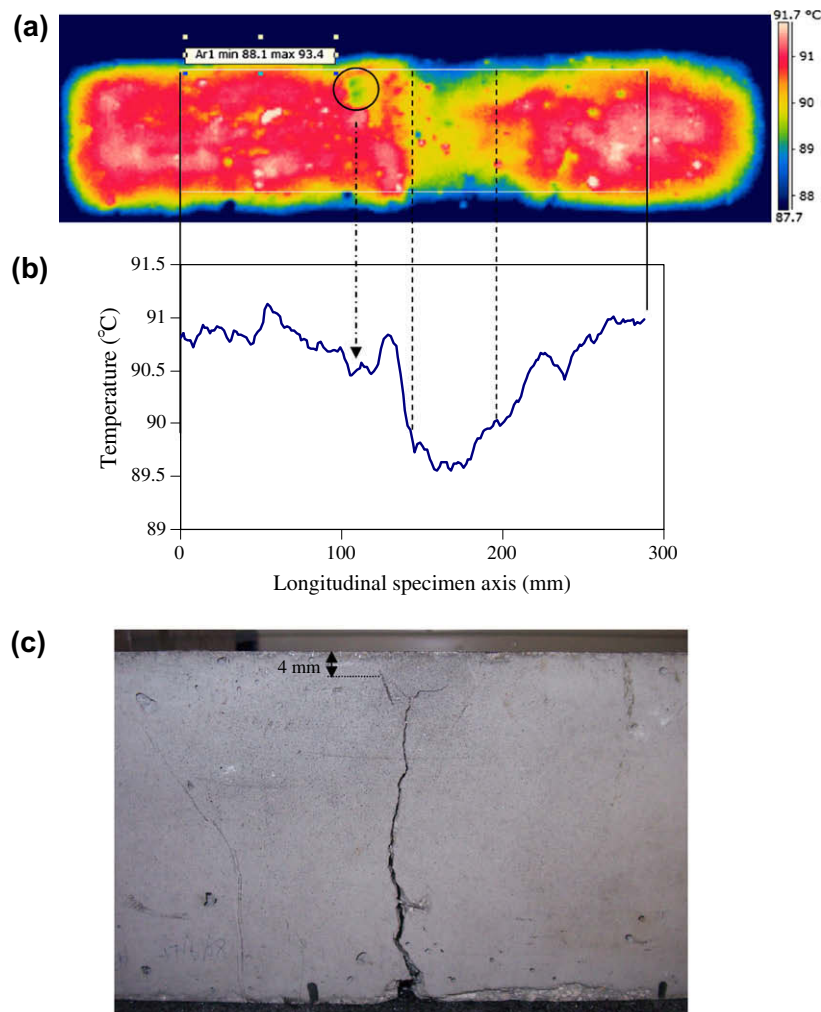


Fig. 11. (a) Thermograph of a specimen with 2 mm center deflection, (b) average temperature for the axis of specimen and (c) side view of the specimen.

line of average temperature will prove useful for the case of subsurface damage, where the anomaly imposed to the temperature field is not much stronger than the anomaly of small surface defects.

Fig. 11a shows the thermograph of a subsurface cracked specimen. The temperature field shows a considerable variation on the area of the defect. In this case the crack corresponds to the middle specimen deflection of 2 mm. For a span of approximately 40 mm the temperature is lower by more than 1 °C than the rest of the specimen. The image by itself is indicative of the subsurface defect area. This can be confirmed by the average temperature line in Fig. 11b that clearly shows a wide local minimum at the area of 150–190 mm, which would be the area to examine by ultrasonic sensors in an actual case. It is mentioned that in certain locations due to small surface anomalies, as indicated by the circle in Fig. 11a, the temperature is similar to the temperature on top of the defect. However, these points create a moderate local minimum on the temperature curve and therefore cannot “mask” the characterization of the defective area. Fig. 11c shows the side view of the specific specimen. The crack split close to the top side

increasing the subsurface anomaly and favoring the characterization by infrared radiation. The crack tip was approximately 4 mm below the surface.

The thermograph obtained for a crack created until the mid span deflection of 1.5 mm, is seen in Fig. 12a. The lower temperature field near the center of the specimen is again visible in the thermograph and the curve of Fig. 12b shows a clear minimum again indicating safely the troublesome area to be examined by ultrasound, although the crack was approximately 8 mm below the surface, as seen in Fig. 12c.

The last case concerns the smallest crack, corresponding to mid span deflection of 1 mm. The temperature field is not clear in this case, since the anomaly imposed by the subsurface defect is less than 1 °C, see Fig. 13a. There are several other fluctuations of the same range and eye examination of the thermograph could lead to different suspicious points due to surface defects. In this case the average curve proves a strong tool because of the sharp local minimum at the position of the defect, which is also global minimum (Fig. 13b). The minimum at 150 mm corresponds to the position of the tip of the crack. The crack tip is approximately

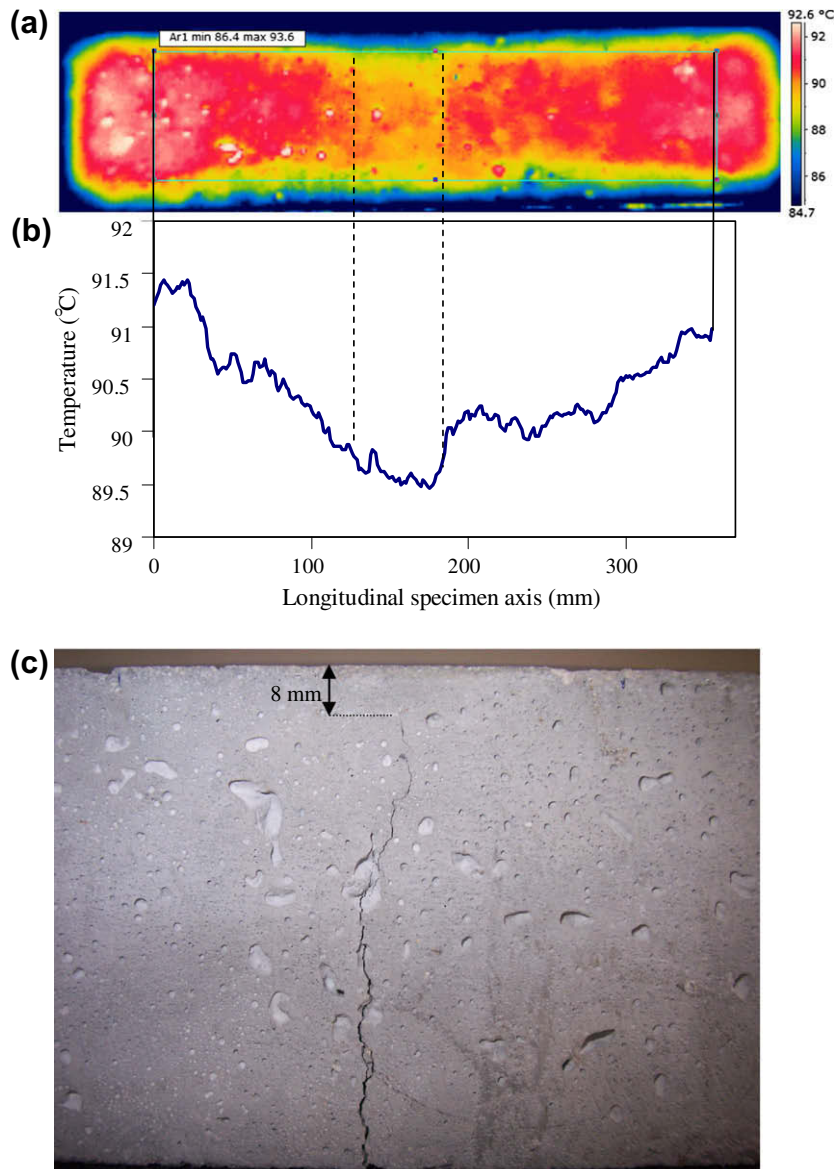


Fig. 12. (a) Thermograph of a specimen with 1.5 mm center deflection, (b) average temperature for the axis of specimen and (c) side view of the specimen.

11 mm below the surface, as seen in Fig. 13c. If another strong minimum is observed, as for instance the minimum on 210 mm in Fig. 13b, the specific position can also be scanned by ultrasonics for safety reasons, since the measurements take just a few minutes. In case there is no subsurface defect this will be safely demonstrated by the wave parameters which will not be influenced.

### 6. Discussion

Some specific points need to be discussed in relation to the applicability of the method in situ. Depending on the internal conditions (e.g. different cover layer), it is possible that corrosion cracking leads to defects parallel to the surface (delaminations) and not vertical cracks as discussed in this study. However, this would make identification easier due to the larger defect area compared to the width of the cracks [5]. Thus, by focusing on the vertical cracking, the method is tuned to identify the least favorable

case, while the characterization capacity for other defect types will be higher. Early identification of the problem will enable the proper action by the engineers which could be epoxy impregnation, or replace of a part of the surface layer [21].

Vertical cracking is of very thin shape (typical crack widths in concrete are less than 1 mm), while the crack tip could be several centimeters below the surface. Therefore, the anomalies which the defect imposes on the temperature field are very weak. In most cases the local minima are just 1 or 2° below the average temperature. Therefore, it is required that the IR camera has a high thermal sensitivity. The IR camera of this study has a sensitivity of 0.06 °C at 30 °C. The small footprint of the defect also requires high temperatures in order to lead to higher heat convection rates and more pronounced differences during the cooling down stage. This was the reason that the specimens were heated up to 90 °C, to initially tune the method. At this temperature range the defects could be identified in laboratory conditions. However, in order to be applicable in actual structures, it would be strongly preferable that the maximum examination temperature would be approximately

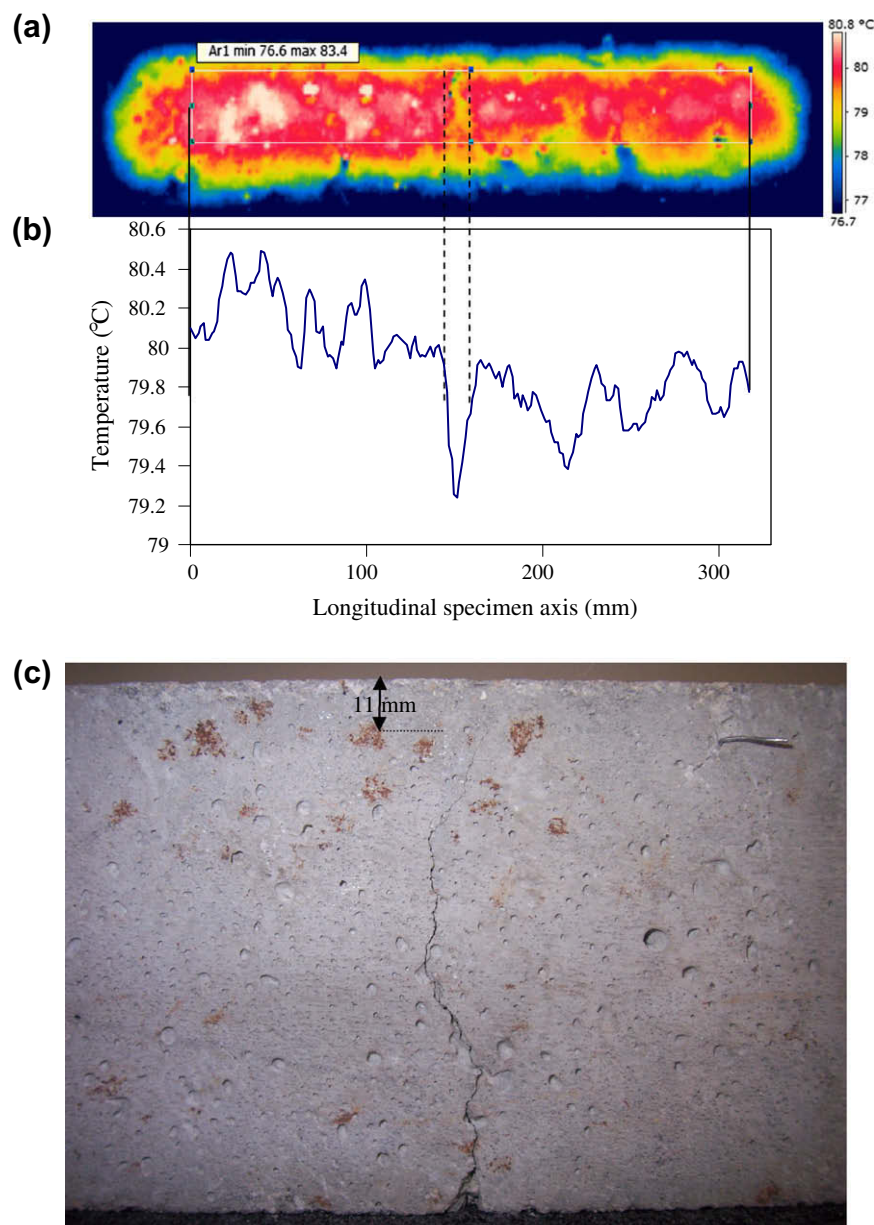


Fig. 13. (a) Thermograph of a specimen with 1 mm center deflection, (b) average temperature for the axis of specimen and (c) side view of the specimen.

50 °C which is a temperature of a concrete surface under sunlight on a warm day. For vertical cracking, the subject needs further investigation. A first try for examination at lower temperatures revealed moderate results as to the identification of the defect. Specifically, the specimens were examined through the IR camera at temperatures around 50 °C. Due to the limited specimen size, the sides lose heat very quickly and therefore, edge effects dominate the heat transfer. Given these circumstances identification of the defects is not an easy task.

Specifically, Fig. 14a shows the thermograph of the specimen with 2 mm deflection and Fig. 14b shows the average temperature line in the white rectangle of Fig. 14a. The drop of temperature is exhibited by the wide minimum around 50 mm. The difference is small but it can be recorded due to the sensitivity of the camera.

Additionally, the specimen with deflection 1.5 mm is depicted in Fig. 15a. Although a sharp minimum is exhibited in the temperature curve of Fig. 15b at 30 mm, which actually corresponds to the position of the crack tip, it is evident that a few centimeters to the left (start of the axis), as well as after 100 mm the temperature decreases due to heat convection from the sides. This demonstrates that larger specimens should be examined in order to exclude the edge effects.

A possible parameter to enhance characterization is the monitoring of the cooling-off curve, which is simply the temperature vs. time function for all the specific points of the mesh. It is possible that the transient thermal image does not show large discrepancies when the crack is small or deep below the surface; however, if the rate of temperature convection is just slightly influenced by

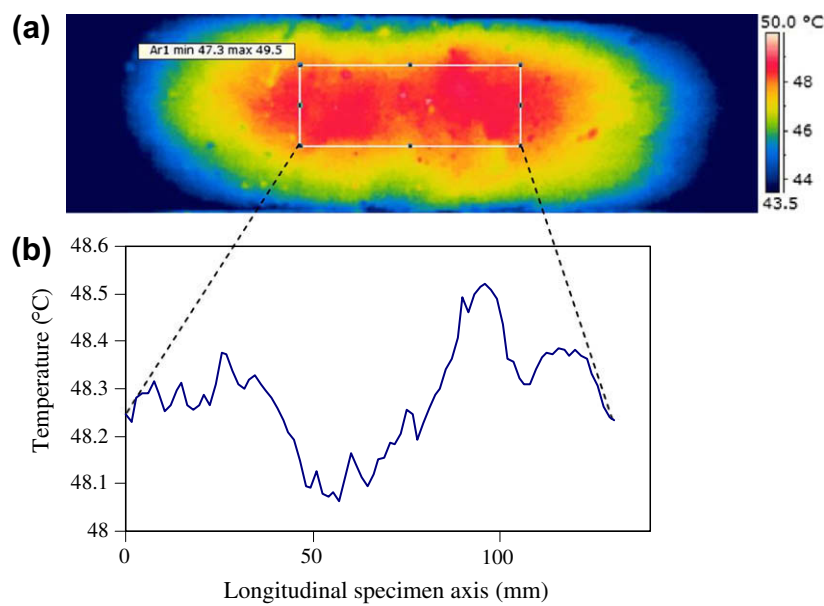


Fig. 14. (a) Thermograph of a specimen with 2 mm center deflection and (b) average temperature for the axis of specimen.

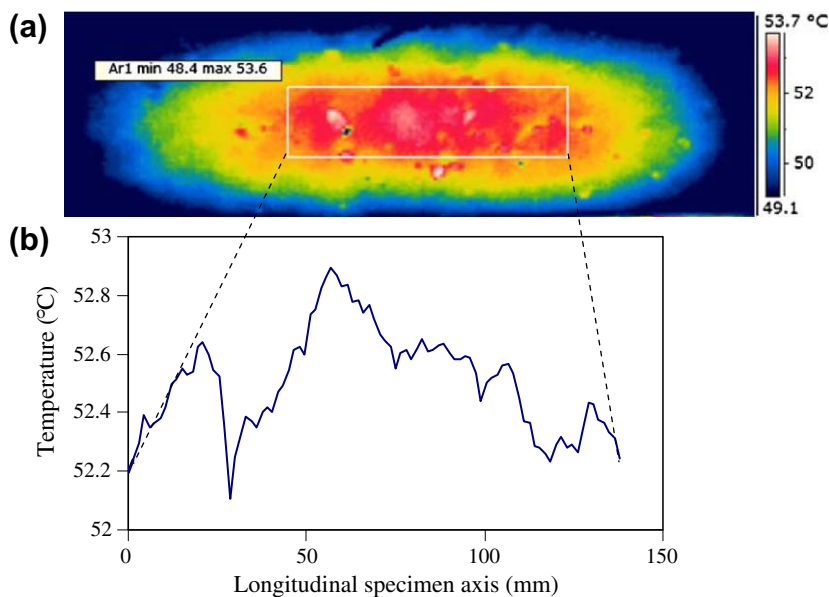


Fig. 15. (a) Thermograph of a specimen with 1.5 mm center deflection and (b) average temperature for the axis of specimen.

the subsurface defect, this would be captured by the cooling-off curve. Alternatively, pulsed or lock-in thermography can be applied by the aid of lamps to provide the necessary heat transfer.

Another important detail that should be taken into account is the direction of heat transfer. In an actual case of a large 3D structure heat convection to air occurs only from the examined surface. In the laboratory case, heat convection occurs also from the sides due to the limited size of the specimens. Additionally, although the crack opening is far away (100 mm on the opposite side of the specimen) it is possible that heat convection from the opposite (tensile) side also influences the obtained thermographs.

Concerning ultrasound, results seem more robust because the crack is vertical to the applied wave propagation. One possible complication is that in cases of severe damage, the Rayleigh waves may not be clearly characterized and thus their velocity will not be measured. Still there is a practical advantage; when subsurface cracking is present, all the complicated mechanisms of reflection, refraction, mode conversion may be active, and their specific contribution on the finally measured wave cannot be clearly identified. However, they result in strong waveform amplitude decrease, giving thus a parameter to correlate with damage regardless of the contribution of each wave mode. An important next step is to use broadband sensors in order to obtain experimental information for different wavelengths. Simulations show that the lowest frequency examined (20 kHz) is the most promising since its transmission seems to be almost linearly dependent to the crack depth up to 60 mm. Attenuation as well as frequency parameters should be focused in order to proceed from the detection of damage to more accurate characterization.

As was already mentioned above, the future actions include use of specimens with larger dimensions, and many different deflection levels, in order to carefully correlate temperature and elastic wave parameters to the imposed damage. Additionally, an IR camera with shorter spectral range (3–6  $\mu\text{m}$ ) will be used in order to capture more detail.

## 7. Conclusions

The present paper occupies with the characterization of subsurface damage in concrete members that could be initiated by metal rebar corrosion and gives no visual sign until cracks break the surface. Steel fiber concrete specimens are scanned by two NDT techniques in order to identify subsurface cracks created by four-point bending. Thermography, as a global and fast technique is used to scan the area under examination, and identify the fingerprint of the defect on the temperature field of concrete surface. For cases of large cracks, the thermal signature on the surface is easily identified on the thermograph; for smaller cracks a simple scheme (based on averaging the temperatures on points on vertical lines of a mesh) leads to correct identification of the damaged area. Consequently one-sided ultrasonic measurements are used to characterize in more detail the depth to crack. The parameter with the highest characterization power seems to be the amplitude of the wave, which reduces by more than 80% in both experiment and simulation, while application of low frequencies (20 kHz) is proposed due to their sensitivity to well hidden cracks below the

surface. The study should continue in order to establish more robust correlations between wave parameters and the depth of the defect since simulations suggest that amplitude parameters are quite promising for subsurface defect characterization. As to thermography, results are encouraging since at high temperatures in laboratory conditions the subsurface defects could be identified in any case, either by the thermograph or by the average temperature curve along the axis of the specimen. However, further work should be done in the identification at lower temperatures in order to challenge the applicability of the method in realistic conditions.

## References

- [1] Muldoon R, Chalker A, Forde MC, Ohtsu M, Kunisue F. Identifying voids in plastic ducts in post-tensioning prestressed concrete members by resonant frequency of impact-echo, SIBIE and tomography. *Constr Build Mater* 2007;21:527–37.
- [2] Shiotani T, Aggelis DG, Makishima O. Global monitoring of large concrete structures using acoustic emission and ultrasonic techniques: case study. *J Bridge Eng - ASCE* 2009;14(3):188–92.
- [3] Ohtsu M, Tomoda Y. Phenomenological model of corrosion process in reinforced concrete identified by acoustic emission. *ACI Mater J* 2008;105(2):194–9.
- [4] Aggelis DG, Shiotani T. Repair evaluation of concrete cracks using surface and through-transmission wave measurements. *Cement Concrete Comp* 2007;29(9):700–11.
- [5] Gary JW. Infrared thermographic techniques. In: Malhotra VM, Carino NJ, editors. *Handbook on nondestructive testing of concrete*. Boca Raton: CRC Press; 1991.
- [6] Maldague X. *Theory and practice of infrared technology for nondestructive testing*. New York: John-Wiley and Sons; 2001.
- [7] Barreira EV, de Freitas VP. Evaluation of building materials using infrared thermography. *Constr Build Mater* 2007;21:218–24.
- [8] Maierhofer C, Brink A, Röllig M, Wiggenhauser H. Detection of shallow voids in concrete structures with impulse thermography and radar. *NDT&E Int*. 2003;36:257–63.
- [9] Naik TR, Malhotra VM. The ultrasonic pulse velocity method. In: Malhotra VM, Carino NJ, editors. *Handbook on nondestructive testing of concrete*. Boca Raton: CRC Press; 1991. p. 169–88.
- [10] Aggelis DG, Momoki S, Chai HK. Surface wave dispersion in large concrete structures. *NDT&E Int*. 2009;42:304–7.
- [11] Liu SW, Sung JC, Chang CS. Transient scattering of Rayleigh waves by surface-breaking and sub-surface cracks. *Int J Eng Sci* 1996;34(9):1059–75.
- [12] Toutanji H. Ultrasonic wave velocity signal interpretation of simulated concrete bridge decks. *Mater Struct* 2007;33:207–15.
- [13] Zerwer A, Polak MA, Santamarina JC. Rayleigh wave propagation for detection of near surface discontinuities: finite element modeling. *J Nondestruct Eval* 2003;22(2):39–52.
- [14] Lomonosov AM, Grigoriev PV, Hess P. Sizing of partially closed surface-breaking microcracks with broadband Rayleigh waves. *J Appl Phys* 2009;105 [art. no. 084906].
- [15] Soulioti D, Barkoula NM, Paipetis A, Matikas TE, Shiotani T, Aggelis DG. Acoustic emission behaviour of steel fibre reinforced concrete under bending. *Constr Build Mater* 2009;23:3532–6.
- [16] Qixian L, Bungey JH. Using compression wave ultrasonic transducers to measure the velocity of surface waves and hence determine dynamic modulus of elasticity for concrete. *Constr Build Mater* 1996;4(10):237–42.
- [17] Selleck SF, Landis EN, Peterson ML, Shah SP, Achenbach JD. Ultrasonic investigation of concrete with distributed damage. *ACI Mater J* 1998;95(1):27–36.
- [18] Aggelis DG, Shiotani T. Experimental study of surface wave propagation in strongly heterogeneous media. *J Acoust Soc Am* 2007;122(5):EL 151–7.
- [19] Wave2000. NY: Cyber-Logic, Inc. (<<http://www.cyberlogic.org>>).
- [20] Kaufman JJ, Luo G, Siffert RS. Ultrasound simulation in bone. *IEEE Trans Ultrason Ferroelectr Freq control* 2008;55(6):1205–18.
- [21] Thanoon WA, Jaafar MS, Razali M, Kadir A, Noorzai J. Repair and structural performance of initially cracked reinforced concrete slabs. *Constr Build Mater* 2005;19(8):595–603.